JSHC
Japan Society of
Histochemistry and Cytochemistry
Established 1959

Acta Histochem. Cytochem. 49 (5): 131–140, 2016
doi: 10.1267/ahc.16020

Roles of Ras Homolog A in Invasive Ductal Breast Carcinoma

Eriko Murakami[1], Yoko Nakanishi[2], Yukari Hirotani[2], Sumie Ohni[2], Xiaoyan Tang[2], Shinobu Masuda[2], Katsuhisa Enomoto[1], Kenichi Sakurai[1], Sadao Amano[1], Tsutomu Yamada[2] and Norimichi Nemoto[2,3]

[1]Department of Breast Surgery, Nihon University School of Medicine, Ohyaguchi-kamimachi, Itabashi-ku, Tokyo 173–8610, Japan, [2]Department of Pathology, Nihon University School of Medicine, Ohyaguchi-kamimachi, Itabashi-ku, Tokyo 173–8610, Japan and [3]Research Institute of Medical Science, Nihon University School of Medicine, Ohyaguchi-kamimachi, Itabashi-ku, Tokyo 173–8610, Japan

Received June 28, 2016; accepted September 16, 2016; published online October 29, 2016

Breast cancer has a poor prognosis owing to tumor cell invasion and metastasis. Although Ras homolog (Rho) A is involved in tumor cell invasion, its role in breast carcinoma is unclear. Here, RhoA expression was examined in invasive ductal carcinoma (IDC), with a focus on its relationships with epidermal-mesenchymal transition (EMT) and collective cell invasion. Forty-four surgical IDC tissue samples and two normal breast tissue samples were obtained. RhoA, E-cadherin, vimentin, and F-actin protein expression were analyzed by immunohistochemistry. *RhoA*, *ROCK*, *mTOR*, *AKT1*, and *PIK3CA* mRNA expression were conducted using laser microdissection and semi-nested quantitative reverse transcription-polymerase chain reaction. RhoA expression was stronger on the tumor interface of IDCs than the tumor center ($P<0.001$). *RhoA* expression was correlated with *ROCK* expression only in HER2-subtype IDC ($P<0.05$). In IDCs co-expressing *RhoA* and *ROCK*, F-actin expression was stronger on the tumor interface, particularly at the edges of tumor cells, than it was in *ROCK*-negative IDCs ($P<0.0001$). In conclusion, RhoA expression was not correlated with EMT in IDC, but enhanced F-actin expression was localized on the edge of tumor cells that co-expressed ROCK. RhoA/ROCK signaling may be associated with collective cell invasion, particularly in HER2-subtype IDC.

Key words: RhoA, invasive ductal carcinoma, F-actin, invasion, EMT

I. Introduction

Breast cancer is the most common female cancer and one of the leading causes of cancer deaths worldwide, accounting for approximately 30% of total new cancer cases in women. The most common causes of cancer death in 2015 were lung and bronchus cancers, followed by breast, colon, and rectal cancers [36]. Although recurrence and metastases after surgical removal of primary tumors are the most common causes of death in breast cancer patients, recent anti-tumor treatment has significantly improved the 5-year survival rate of breast cancer patients [21]. The precise mechanisms of metastasis in breast cancer are complicated, and many proteins and signaling pathways are involved in the process [6].

Cancer progression is thought to begin when a single cell invades via amoeboid movement or undergoes a phenotypic change called the epithelial-mesenchymal transition (EMT) and begins to invade the surrounding primary tumor mass, including as tumor buds [14, 15]. EMT is a naturally inherited cellular program required during the developmental processes of embryogenesis and tissue remodeling and is an acquired function in malignant neoplasms [27]. *In vitro* studies on cancer cell lines in human and mouse models have suggested that the aberrant activation of EMT is involved in tumor cell dissemination and

Correspondence to: Yoko Nakanishi, Department of Pathology, Nihon University School of Medicine, 30–1 Ohyaguchi-kamimachi, Itabashi-ku, Tokyo 173–8610, Japan. E-mail: nakanishi.youko@nihon-u.ac.jp

metastases via the blood stream [6, 19, 35]. In addition, the role of EMT in circulating tumor cells has been investigated [41]. On the other hand, the invasion of tumor cell masses without EMT has been reported. In these cases, cohesively accumulated tumor cells may contribute to the mechanism of invasion [9]. Although EMT is one theory explaining tumor invasion and metastasis [35], most invasive solid tumors display predominantly collective migration and invasion, in which groups of cells invade the peritumoral stroma while maintaining cell-cell contacts, and expansive growth, which is proposed to characterize whole tumor tissue dynamics [9]. Cells lose the cell-cell junctions and apical-basal polarity during EMT, and many polarity proteins relocate toward the leading edge to induce a polarity consisting of a front side and a rear side of cells [31]. Such polarity differences might result from the differential expression of surface receptors in the front cells compared with the rear cells [3, 35]. Cancer cell groups, which are called collective cells, are thought to be heterogeneous and include cells that are leaders and cells that are followers [38]. In whole tumor tissue, Ki67 staining was used to demonstrate an increase in proliferation at the tumor/stromal interface compared with the tumor center [14]. The biological behavior of cancer is thought to be more accurately reflected by the histological features present at the invasive front rather than those observed at the tumor center [12].

The dynamics of the cytoskeleton, cell migration, malignant transformation, cell polarity, invasion, and metastasis are regulated by Ras homolog (Rho) GTPases [17, 28], and the overexpression of these proteins has been observed in various human neoplasms showing aberrant regulatory mechanisms [17]. The Rho subfamily of low-molecular-mass GTP-binding proteins encompasses RhoA-like (e.g., RhoA, B, and C), Rac, and Cdc42 proteins [10]. RhoA overexpression has been demonstrated in various tumor types, such as testicular, breast, colon, lung, and liver cancers [1, 10, 11, 13, 20]. RhoC is also overexpressed in various tumors [28]. RhoB expression is not only overexpressed, but also reportedly exhibits downregulation and the loss of expression in some neoplasms [13, 25, 28, 33]. It is thought that RhoB has opposite functions in tumor progression and suppression. Orgaz *et al.* presented a diagram that summarizes different roles of GTPases during cell transformation and tumor progression [28]. During the process of progression to premalignant conditions, Rho GTPases are involved in aberrant proliferation, altered metabolism, cell survival, the inhibition of senescence, and apoptosis. At non-invasive stages (*in situ* carcinoma), Rho GTPases enhance inflammation and stimulate cell proliferation, cell survival, and tumor angiogenesis. At the later stage of tumorigenesis, Rho GTPases contribute to the rearrangement of cytoskeletons, cell motility, migration, and invasion. RhoA induces cell migration, invasion, and metastasis via the activation of F-actin [40]. Lin *et al.* showed that caveolin 1 (Cav1) links the mechanical phenotype to cancer cell transformation and is involved in RhoA activation and ^{Y397}FAK phosphorylation, which are both required for actin cap formation in fibroblasts, using various cancer cell lines [22]. Cytochalasin D (CytD), an actin binding inhibitor, reduces cell size and F-actin expression levels via the inhibition of active RhoA [33]. Although RhoA signaling plays a key role in cancer cell invasion and metastasis, EMT, PI3K/AKT/mTOR signaling, and increasing F-actin expression are also closely related to the progression of breast carcinomas. In this study, we clarified the role of RhoA expression in human breast carcinoma expanding growth.

II. Materials and Methods

Patients

Forty-four patients who were diagnosed with primary invasive breast carcinoma and underwent a modified radical mastectomy at Nihon University Itabashi Hospital between 2003 and 2008 were recruited. The Institutional Review Board of Nihon University Itabashi Hospital approved this retrospective study. The patients did not receive any anti-tumor therapies before surgery. Two patients with benign breast lesions were included as normal controls. A summary of the patient characteristics is presented in Table 1. All surgical specimens were routinely fixed with 20% formalin and embedded in paraffin. The statuses of estrogen receptor (ER), progesterone receptor (PgR), and human epidermal growth factor receptor (Her) 2 were routinely examined to determine the breast carcinoma subtype.

Immunohistochemistry

Immunohistochemistry (IHC) was performed on 4-μm formalin fixed and paraffin embedded (FFPE) tissue sections. In the E-cadherin IHC procedure, after the tissue sections were dewaxed, they were autoclaved in EDTA buffer (pH 9.0) for 15 min at 121°C for antigen retrieval and cooled at room temperature. After washing them several times in phosphate-buffered saline (PBS) (pH 7.2), the sections were processed to quench endogenous peroxidase activity with 0.3% hydrogen peroxide and to block non-specific binding with 1% goat serum. The sections were then incubated with the primary antibody, anti-mouse monoclonal E-cadherin antibody (Clone HECD-1, 1:100; Takara Bio Inc., Kusatsu, Shiga, Japan), for 30 min at room temperature. After washing with PBS, the sections were reacted with the SimpleStain MaxPO Multi Polymer System (Nichirei Biosciences Inc., Tokyo, Japan). For Vimentin IHC, antigen retrieval was performed using a microwave in citrate buffer (pH 6.0). The primary antibody was anti-rabbit monoclonal Vimentin antibody (Clone SP20, ×1, Nichirei Biosciences Inc.), and the SimpleStain MaxPO Multi Polymer System (Nichirei Biosciences Inc.) was used. For RhoA and F-actin IHC, antigen retrieval was performed by autoclaving in citrate buffer (pH 6.0). The

Table 1. *Summary of the patients*

Category	Number of patients
Histology	
Papillotubular carcinoma	23
Solid-tubular carcinoma	9
Scirrhous carcinoma	11
Mixed type	1
Age	
<35	3
35≤	41
Stage	
I	22
II	11
III	11
Tumor size (cm)	
≤2	27
>2; ≤5	13
>5	4
Lymph node status	
Negative	27
Positive	12
No information	5
Hormone receptor	
ER (+), and/or PgR (+), Her2 (−)	13
ER (−), PgR (−), Her2 (+)	13
ER (−), PgR (−), Her2 (−)	18
Normal breast tissues	2
Total	46

primary antibodies were anti-mouse monoclonal RhoA antibody (Clone 26C4, 1:100; Santa Cruz Biotechnology, Inc., Dallas, TX, USA) and anti-rabbit polyclonal F-actin antibody (1:300; Bioss Inc., Woburn, MA, USA). The SimpleStain MaxPO Multi Polymer System (Nichirei Biosciences Inc.) was used as the secondary antibody. Immunohistochemical procedures were performed using automated staining equipment (Histostainer; Nichirei Biosciences Inc.). As positive controls, the following tissues were used: colon carcinoma for E-cadherin, malignant mesothelioma for vimentin, cervical cancer for RhoA, and endothelial cells for F-actin [16]. For negative controls, the primary antibodies were omitted, and samples were incubated with dilution buffer. Tissue-bound HRP activity was visualized by immersing the sections in 0.005% 3,3'-diaminobenzidine tetrahydrochloride (DAB) in PBS containing hydrogen peroxide (10 μL/150 mL DAB solution). Each section was counterstained with hematoxylin. Immunohistochemical intensity scores were evaluated as negative (0), weak (1+), moderate (2+), and strong (3+) at the tumor interface and the tumor center. The tumor interface region was evaluated using 0.5 mm to 1.0 mm of the surrounding side of the primary whole tumor tissue, and the tumor center was evaluated using a section approximately 1.0 mm in diameter (Fig. 1).

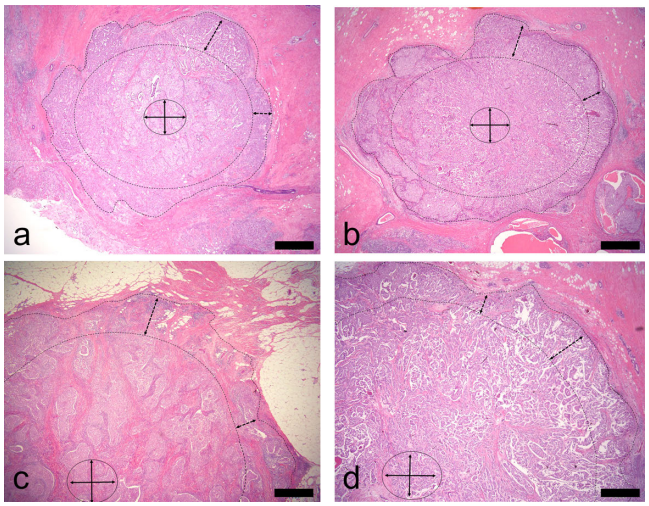

Fig. 1. Tumor interface and tumor center are shown (×2). (**a**) and (**b**) are tumor masses smaller than 20 mm in diameter. (**c**) and (**d**) are tumor masses larger than 20 mm in diameter. Tumor cells in an area approximately 1 mm from the edge of the tumor mass (enclosed by dotted line) were investigated as the tumor interface, and cells in the center of the tumor mass were investigated as the tumor center. All sections were stained with hematoxylin and eosin. Bar=1 mm.

Immunofluorescence

The sections (4-μm thick) were dewaxed with xylene and dehydrated in a graded ethanol series. Formalin was then eliminated by treatment with 5% ammonia and 95% ethanol for 30 min at room temperature. For antigen retrieval, the tissue sections were autoclaved in citrate buffer (pH 6.0) for 15 min at 121°C and cooled at RT. After washing, sections were incubated with the three mixed primary antibodies, including the anti-mouse monoclonal RhoA antibody (Clone 26C4, 1:100; Santa Cruz Biotechnology, Inc.) and anti-rabbit polyclonal F-actin antibody (1:300; Bioss Inc.) for 30 min at room temperature. After washing with PBS, sections were incubated with Alexa Fluor 488-labeled anti-rabbit IgG in goat serum (1:500, Thermo Fisher Scientific Inc., Waltham, MA, USA) and Alexa Fluor 594-labeled anti-mouse IgG with goat serum (1:500, Thermo Fisher Scientific Inc.) for 30 min at room temperature. After washing with PBS, sections were mounted with ProLong Diamond Antifade Mountant with DAPI (Thermo Fisher Scientific Inc.). Images were acquired using an Olympus IX71 fluorescence microscope (Olympus Corp., Tokyo, Japan) and color images were obtained using Lumina Vision software (Mitani Co., Tokyo, Japan).

Total RNA extraction from microdissected tumor tissue

The 8-μm-thick FFPE sections were mounted on membrane film-coated slides. After dewaxing with xylene, the sections were lightly stained with toluidine blue. The target tumor areas were then microdissected using a laser-assisted microdissection system (PALM MBIII-N; Zeiss, Jena, Germany). The microdissected target tumor cells were retrieved precisely and placed in an Eppendorf lid

Table 2. *Real-time RT-PCR primer sequences*

Target	Forward primer	Reverse primer	Tm* (°C)	Product size (bp)
RohA	5'-cgcttttgggtacatggagt-3'	5'-caagacaaggcacccagatt-3'	60.0	124
ROCK	5'-cttttgccaacagtccttggg-3'	5'-acaagatctccaccaggcatg-3'	60.0	100
PIK3CA	5'-ctctgcaaaaaggccactgt-3'	5'-gccgtaaatcatccccattt-3'	60.4	107
AKT1	5'-gcaccttccatgtggagact-3'	5'-tgagttgtcactgggtgagc-3'	60.1	130
mTOR	5'-ttaatggaggcccaagagtg-3'	5'-gctttgagattcgtcggaac-3'	60.1	109
GAPDH	5'-ggaaggtgaaggtcggagtca-3'	5'-gtcattgatggcaacaatatccact-3'	60.0	101

*Tm: melting temperature

with mineral oil. The laser-assisted microdissection procedures have been previously described [26]. Additionally, benign mammary epithelial cells were microdissected from two breast cancer tissue sections. Total RNA was extracted as previously described [24, 26, 39].

The target tumor cell sample was mixed with 200 μL of denaturing buffer containing 2% SDS, 0.1 mM EDTA, and 10 mM Tris-HCl. The samples were then incubated at 55°C with proteinase K until sections were completely dissolved. Total RNA was purified with 20 μL of 2 M sodium acetate (pH 4.0), 220 μL of citrate saturated phenol (pH 4.3), and 60 μL of chloroform-isoamyl alcohol, centrifuged for 15 min at 15,000 rpm, and the upper aqueous layer was transferred to new tubes. Two hundred microliters of isopropanol and 2 μL of glycogen were added as a carrier and the samples were stored at −80°C for more than 30 min, centrifuged at 14,000 rpm, washed with 70% ethanol, and air dried on ice. They were then dissolved in 5–10 μL of RNase-free water and quantified by measuring the optical density at 260 nm using the NanoDrop 1000 (Thermo Fisher Scientific Inc.). Total RNA samples were stored at −80°C until use. Both genomic DNA elimination and cDNA synthesis were performed using the QuantiTect Reverse Transcription Kit (QIAGEN, GmbH, Hilden, Germany) according to the manufacturer's instructions.

Real-time RT-PCR

The mRNA levels of *RhoA*, *Rock*, *PI3K*, *AKT*, *mTOR*, and glyceraldehyde 3-phosphate dehydrogenase (*GAPDH*) as an internal control were measured using quantitative semi-nested real-time polymerase chain reaction (snqRT-PCR) methods [1, 11, 13, 25, 33]. The first RT-PCR reaction was carried out with each target and control cDNA using the AmpliTaq Gold® 360 Master Mix (Thermo Fisher Scientific Inc.) and the respective primers shown in Table 2. Samples were incubated at 95°C for 10 min before they were subjected to 25 cycles of denaturation at 94°C for 30 sec, annealing at 60°C for 30 sec, and extension at 72°C for 1 min. The first reaction was performed on a conventional PCR machine (PC808; ASTEC Co. Ltd., Fukuoka, Japan). Two microliters of each resulting product was used as the template in the second snqPCR amplification, which was performed using the StepOnePlus™ Real-time PCR System (Thermo Fisher Scientific Inc.) with Power SYBR® Green detection chemistry (Thermo Fisher Scientific Inc.). Briefly, snqPCR amplification was performed in a 20-μL final reaction volume containing 900 nmol/L each primer used in the first RT-PCR reaction (Table 2) and 1× Power SYBR® Green PCR Master Mix (Thermo Fisher Scientific Inc.). The reaction mixture was preheated at 95°C for 10 min, followed by 40 cycles of 95°C for 15 sec and 60°C for 1 min. Relative target mRNA values were obtained using the ΔΔCt method [23].

Statistical analysis

The significance of the differences in *RhoA* mRNA expression levels with respect to clinicopathological status and location (i.e., between the invasive front and core side) in IDC tissues were evaluated using the Mann-Whitney U test. The correlation between intrinsic IDC subtypes and *RhoA* mRNA expression levels was analyzed. A multivariate analysis and Kaplan-Meier log-rank tests were performed. All statistical analyses were performed using SPSS® Statistics version 20.0 (IBM Japan, Tokyo, Japan).

III. Results

Immunohistochemical expression of RhoA and F-actin

Immunohistochemically, RhoA was expressed in the cytoplasm of all IDCs and almost all tumor cells were RhoA-positive (Fig. 2a). E-cadherin and vimentin expression levels were investigated to clarify the correlation between RhoA expression and EMT in tumor cells. E-cadherin was expressed in the tumor cell membranes (Fig. 2b) of 81.8% (36/44) of samples. Vimentin was not expressed in the tumor cells of any IDCs (Fig. 2c). F-actin was also expressed in all IDCs and its expression was localized to the tumor cell membrane, cytoplasm, and extracellular matrix (Fig. 2d). In normal mammary gland cells, RhoA was not expressed (Fig. 2e) and E-cadherin was expressed in the cell membrane (Fig. 2f). Vimentin and F-actin were not expressed in normal mammary gland cells (Fig. 2g and 2h, respectively).

RhoA and F-actin were expressed at various intensities, even within the same tumor tissue section (Fig. 3a, 3d, respectively), from weak expression (1+, Fig. 3b, 3e, respectively) at the tumor center to strong expression (Fig. 3c, 3f, respectively) at the tumor interface of each tumor.

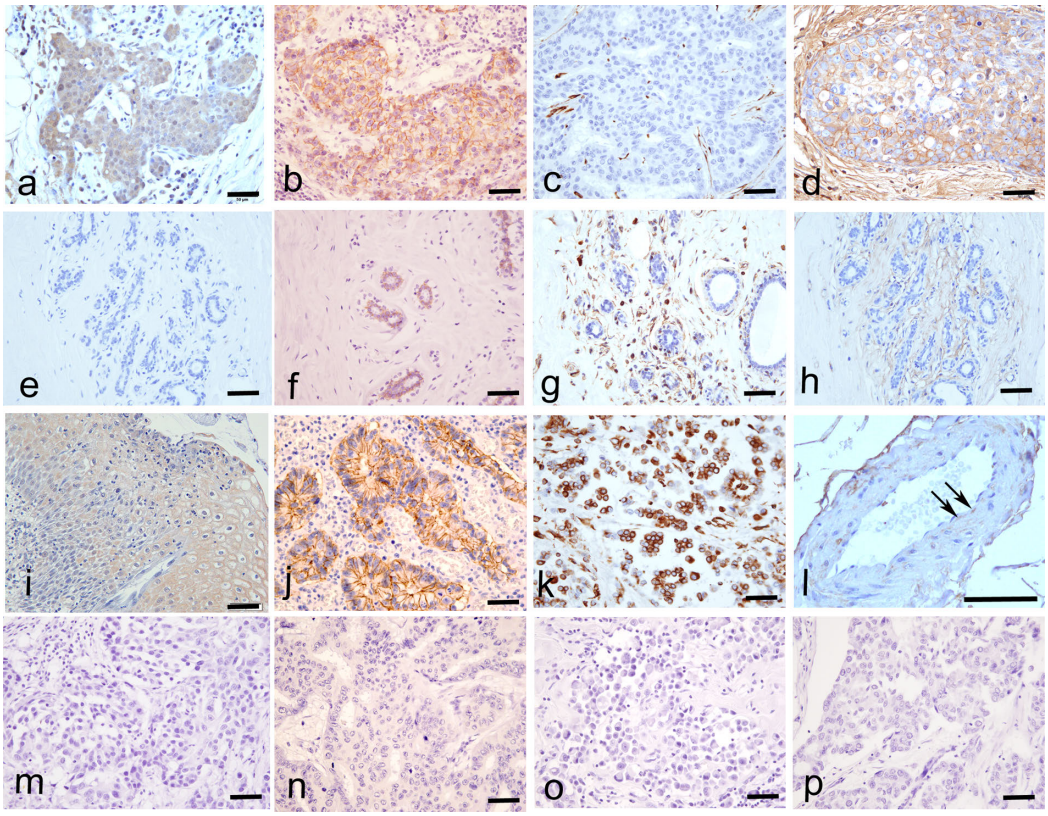

Fig. 2. Immunohistochemical expression of RhoA, E-cadherin, vimentin, and F-actin (×40). RhoA was expressed in the tumor cytoplasm based on immunohistochemistry in IDC (**a**), but not in normal breast tissues (**e**), in cervical cancer as a positive control (**i**), and in the negative control (**m**). E-cadherin was expressed in the tumor cell membrane in IDC (**b**) and in normal breast tissues (**f**), in colon cancer as a positive control (**j**), and in the negative control (**n**). Vimentin was not expressed in any IDC samples (**c**), normal breast tissues (**g**), in malignant mesothelioma as a positive control (**k**), and in the negative control (**o**). F-actin was expressed in the extracellular matrix of tumor cells and/or the tumor cell membrane (**d**), in normal breast (**h**), in endothelial cells (**l**, arrow) as a positive control, and the negative control (**p**). Bar=50 μm.

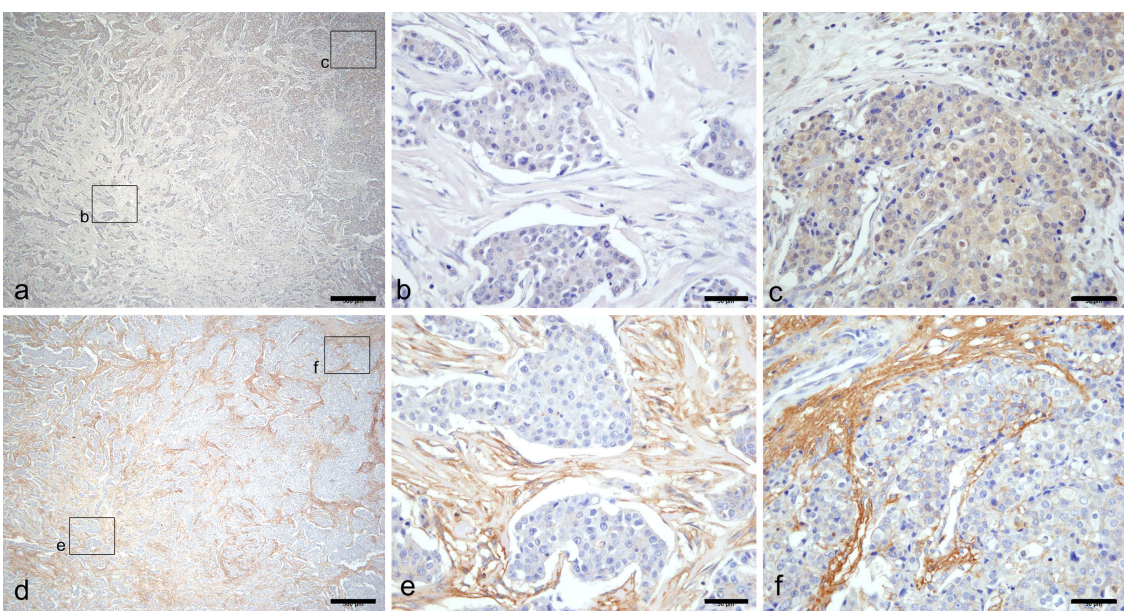

Fig. 3. Immunohistochemical localization of RhoA and F-actin. Heterogeneous expression of RhoA (**a**) and F-actin (**d**) are shown. Weak expression of both RhoA (**b**) and F-actin (**e**) were detected on the tumor center, and stronger expression of both RhoA (**c**) and F-actin (**f**) were detected on the tumor interface. Bar=500 μm (**a, d**), 50 μm (**b, c, e, f**).

RhoA protein and mRNA expression on the front side and the core side of IDC

The RhoA IHC expression level was significantly higher on the tumor interface than the tumor center (P<0.001, Fig. 4a). Therefore, mRNA expression levels in samples extracted from microdissected tumor cells on the tumor interface and tumor center were analyzed. The *RhoA* mRNA expression level, standardized by the *GAPDH* mRNA expression level, did not differ significantly between the tumor interface and tumor center (Fig. 4b), in contrast to the immunohistochemical protein localization.

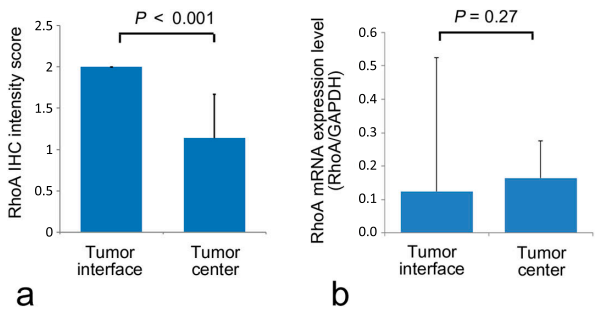

Fig. 4. Immunohistochemical RhoA expression levels (**a**) and *RhoA* mRNA expression levels (**b**) on the tumor interface and the tumor center were measured. The immunohistochemical intensity score was significantly higher on the tumor interface than the tumor center (P<0.001). There were no significant differences of *RhoA* mRNA expression levels, however, between the tumor interface and the tumor center.

RhoA mRNA expression levels and clinicopathological features

The correlations between *RhoA* mRNA expression levels, standardized by *GAPDH* expression, and clinicopathological features of IDCs are summarized in Table 3. *RhoA* expression was significantly higher in breast carcinoma samples than in normal mammary glands (P=0.006). In IDC samples, papillotubular carcinoma and scirrhous carcinoma samples exhibited significantly higher RhoA expression levels than solid tubular carcinoma samples (P=0.04). Stage II and III tumors exhibited significantly higher RhoA expression than stage I tumors (P=0.02), but the *RhoA* mRNA expression level was not correlated with tumor size. The correlation between *RhoA* mRNA expression level and the receptor status of IDCs was investigated. The ER(−), PgR(−), HER2(−) subtype exhibited signifi-

Table 3. *RhoA mRNA expression levels and clinicopathological features*

Categories	Number of cases	*RhoA* mRNA expression level Mean±SD	*P*-value
Normal breast tissue	2	0.01±0.01	0.006
Total of IDC	44	0.06±0.15	
Histology			
Solid tubular carcinoma	9	0.05±0.05	
Papillotubular carcinoma	23	0.10±0.08	0.04
Scirrhous carcinoma	11	0.11±0.13	
Mixed type	1		
Stage			
I	22	0.07±0.06	
II	11	0.16±0.16	0.02
III	11	0.11±0.08	
Tumor size (cm)			
≤2	27	0.09±0.09	
>2, ≤5	13	0.10±0.13	N.S.
>5	4	0.15±0.07	
Hormone receptor status			
ER (+) and/or PgR (+), Her2 (−)	13	0.10±0.10	*0.08
ER (−) and PgR (−), Her2 (+)	13	0.15±0.13	**0.02
ER (−) and PgR (−), Her2 (−)	18	0.06±0.08	
Lymph node status			
Negative	27	0.09±0.05	
Positive	12	0.14±0.12	0.08
No information	5		
Prognosis			
No recurrence	31	0.10±0.11	
Recurrence	5	0.10±0.11	N.S.
Death from tumor	4	0.05±0.09	
No information	4		

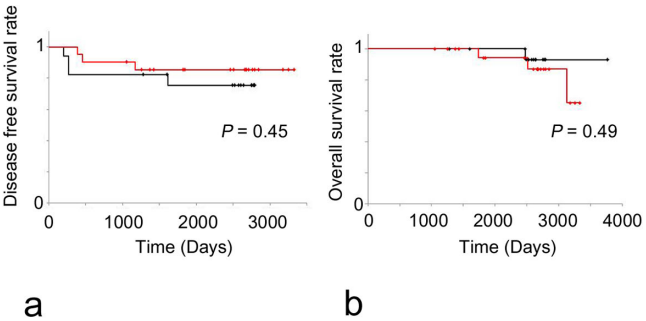

Fig. 5. Prognostic analyses of the IDC patients classified according to *RhoA* mRNA expression levels. (**a**) Disease-free survival rate (DFS) was not significantly different between the high *RhoA* mRNA expression group (black) and the low *RhoA* mRNA expression group (red) based on a log-rank test. (**b**) Overall survival rate (OS) was not significantly different between the high *RhoA* mRNA expression group (black) and the low *RhoA* mRNA expression group (red) based on a log-rank test.

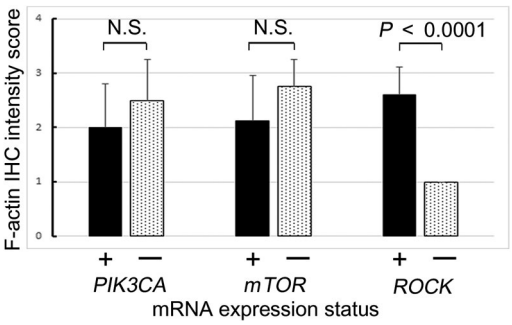

Fig. 6. Immunohistochemical F-actin intensity score in tumor cells evaluated as negative (0), weak (1+), moderate (2+), and strong (3+) for tumors with *RhoA* overexpression. The *x*-axis shows the expression status of each target mRNA.

cantly lower *RhoA* mRNA expression levels than the ER(−), PgR(−), HER2(+) subtype (P=0.02), and tended to have lower expression than the ER(+), PgR(+), HER2(−) subtype (P=0.08). No significant difference was found between the ER(−), PgR(−), HER2(+) subtype and the ER(+), PgR(+), HER2(−) subtype. Lymph node metastasis-positive tumors tended to have higher *RhoA* mRNA expression levels than lymph node metastasis-negative tumors (P=0.08). Patient prognosis was not correlated with *RhoA* mRNA expression level. Based on a Kaplan-Meier analysis, the *RhoA* mRNA expression level was not correlated with disease-free survival time or overall survival time for the IDCs (Fig. 5a, b).

Correlations between RhoA mRNA expression and PIK3CA, AKT1, mTOR, and ROCK mRNA expression

In the present study, the mRNA expression levels of *PIK3CA*, *AKT1*, *mTOR*, and *ROCK* were measured to investigate their correlations with *RhoA* expression levels for every receptor status subtype, and the results are shown in Table 4. In the ER(−), PgR(−), HER2(+) subtype, the correlation coefficients for the relationships of *mTOR* and *ROCK* with *RhoA* mRNA expression levels were 0.86 (P=0.007) and 0.85 (P=0.01), respectively. In the ER(+), PgR(+), HER2(−) subtype, no correlation between the target mRNA and *RhoA* mRNA expression levels were detected. Although for the ER(−), PgR(−), HER2(−) subtype and total cases the correlation coefficients for *PIK3CA* and *RhoA* mRNA expression levels were 0.69 (P=0.02) and 0.88 (P<0.0001), respectively, these results were derived from negative correlations.

Correlation between combined PIK3CA/RhoA, mTOR/RhoA, and ROCK/RhoA mRNA expression and F-actin protein expression

RhoA mRNA expression levels were correlated *PIK3CA*, *mTOR* and *ROCK* mRNA expression levels. Therefore, the correlation between F-actin IHC intensity score, which was the sum of the stromal fibroblastic intensity score and tumor cell membranous intensity score, was investigated. In the sample with co-expression of *RhoA* and *ROCK* mRNA, the F-actin IHC score was significantly higher than that of the *RhoA*-positive, but *ROCK*-negative sample (P<0.0001, Fig. 6).

In IDC samples that co-expressed *RhoA* and *ROCK* mRNA, both RhoA and F-actin were overexpressed in each tumor cell (Fig. 7). F-actin was mainly localized at the edge of each tumor cell with cytoplasmic RhoA overexpression. However, the signals of F-actin and RhoA were not strictly co-expressed.

Table 4. *Correlation coefficients for relationships between RhoA mRNA expression levels an PIK3CA, AKT1, mTOR, and ROCK based on a multivariate analysis*

mRNA	Receptor status			Total
	ER (+), PgR (+), Her2 (−)	ER (−), PgR (−), Her2 (+)	ER (−), PgR (−), Her2 (−)	
PIK3CA	−0.13	0.19	0.69*	0.88**
AKT-1	0.33	0.16	−0.50	0.01
mTOR	0.31	0.86*	0.49	0.26
ROCK	0.10	0.85*	0.05	0.26

*: P<0.05, **: P<0.0001.

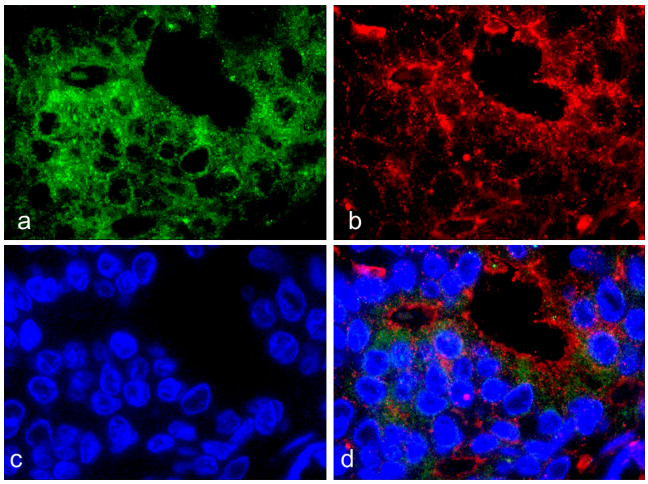

Fig. 7. Immunofluorescence staining of IDC showed the expression patterns of RhoA and F-actin. (×100 oil). **a:** RhoA (Alexa Fluor 594, green), **b:** F-actin (Alexa Fluor 488, red), **c:** DAPI, **d:** merged fluorescent images.

IV. Discussion

The significance of RhoA expression in invasive breast carcinoma was investigated with respect to three mechanisms, EMT, PI3K/AKT/mTOR signaling, and increases in F-actin expression. Rho GTPases regulate cytoskeleton dynamics, cell migration, malignant transformation, cell polarity, invasion, and metastasis [17, 28], and the overexpression of these proteins has been observed in various human neoplasms, suggesting aberrant regulatory mechanisms [17]. Poor prognosis in breast cancer is attributed to invasion and metastases, particularly distant metastases [2, 7, 34]. EMT is one theory explaining tumor invasion and metastasis [35]. Although RhoA activation downregulates E-cadherin expression and induces EMT in metastatic cancer cells [33], the correlation between RhoA expression and EMT, which is suggested by the negative E-cadherin expression and the positive vimentin expression, has not been found. The metastatic process comprises an ordered series of events in which the acquisition of a motile and invasive phenotype to penetrate the ECM is an important determinant of the invasive potential of tumor cells [2, 4]. Actin polymerization (F-actin), which is induced by RhoA, a small GTPase, is involved in cell migration in a breast cancer cell line [2]. The mechanisms of Rho regulation, including a kinase cascade triggered by growth factor stimuli and integrin-ECM interaction-mediated focal adhesion and stress fiber formation, have been described [5]. In addition, the integrin-ECM interaction has been shown in the tip cells at the invasive front of vascular sprouting, multicellular masses, and detached cancer cells [8]. Several mechanisms polarize the cell cohort into "leader" or "pioneer" cells that guide "followers" at their rear [37]. This front-rear asymmetry is a feature of all migrating collectives described to date. Leader cells in the front row or "tip" display distinct, polarized morphologies, detect extracellular guidance cues, and generate stronger cytoskeletal dynamics than follower cells in the cohort [37]. In the present results, RhoA and F-actin protein expression levels were different between the tumor interface and tumor center, although their mRNA expression levels were not significantly different. Therefore, not only single cell and cell cluster polarity but also tumor mass polarity may contribute to whole tissue dynamics by RhoA/ROCK signaling. Stromal cell derived factor-1α (SDF-1α) is expressed with its chemokine receptor CXCR4 in mesenchymal stromal cells of metastatic tumors and modulates tumor cell migration via F-actin stress fiber and filopod formation after RhoA activation [29]. In this study of IDC patients, however, RhoA expression did not always induce F-actin overexpression in IDC. In tumors with *RhoA* and *ROCK* mRNA co-expression, in particular, F-actin protein expression was higher than that in other samples expressing *RhoA*. Co-expression of *RhoA* and *ROCK* mRNA was found in only ER(−), PgR(−), and HER2(+) subtype with a significantly higher correlation. However, higher *RhoA* mRNA expression was not correlated with disease-free survival or overall survival. IDC cases with higher *RhoA* expression tended to have relapses (not significant), but better prognoses (not significant). As HER2-positive IDC patients were provided effective targeted molecular therapy using trastuzumab, their overall survival may have been better than that of other patients. Triple negative IDC samples, i.e., those that were ER(−), PgR(−), and HER2(−), exhibited the lowest *RhoA* mRNA expression. Accordingly, the correlation between low *RhoA* and low *PIK3CA* mRNA expression levels appeared to be strong. *PIK3CA* mRNA expression combined with *RhoA* mRNA overexpression was not associated with F-actin overexpression. *mTOR* mRNA expression levels were also not correlated with F-actin protein expression levels via *RhoA* mRNA overexpression. The Rho/Rock signaling pathway is involved in lysophosphatidic acid-induced breast cancer cell invasion via MMP activation [34], and regulates three-dimensional cell migration by matrix reorganization [30]. Different modes of tumor cell invasion have distinct requirements for Rho/ROCK signaling and extracellular proteolysis has been reported [18]. These studies of evidence reveal the mechanisms of tumor invasion of the surrounding tissue. These results show that RhoA/ROCK signaling may be required for expanding tumor growth including collective cancer cell invasion via extracellular proteolysis and reorganization by F-actin polymerization localized to the IDC edge, particularly in the HER2 subtype. The molecular mechanism for expanding growth and invasion in the luminal subtype, which is ER(+), PgR(+), and HER2(−), and the triple negative subtype, which is ER(−), PgR(−), and HER2(−), of IDC might be different from RhoA/Rock signaling. HER2 overexpression may trigger the acceleration of cell invasion and proliferation of tumor cells, not only by fibronectin [18] but also by RhoA/ROCK signaling. The inhibi-

tion of Rho or ROCK function was not effective against the movement of cells with an elongated morphology; this may promote selection for cells that use this mode of mobility [32]. The expression patterns of RhoA and ROCK were heterogeneous in IDCs, and the tumors with F-actin overexpression via RhoA and ROCK co-expression should be selected to effectively inhibit these mechanisms.

V. Conclusions

RhoA expression was heterogeneous in IDC; expression was lower on the tumor center and higher on the tumor interface. RhoA was not correlated with EMT, as predicted by the invasion theory, in IDC, but enhanced F-actin expression was localized to the edges of tumor cells with ROCK co-expression. RhoA/ROCK signaling and tumor mass polarity may be associated with expanding growth including collective cell invasion as tumor buds, particularly in the HER2 subtype of IDC.

VI. Acknowledgments

We wish to thank Ms. Ai Itoh (Department of Pathology, Nihon University School of Medicine) and Ms. Mayumi Katsunuma (Department of Pathology, Nihon University School of Medicine) for their technical assistance, including immunohistochemistry and immunofluorescence.

VII. References

1. Adnane, J., Muro-Cacho, C., Mathews, L., Sebti, S. M. and Nunoz-Antonia, T. (2002) Suppression of rho B expression in invasive carcinoma from head and neck cancer patients. *Clin. Cancer Res.* 8; 2225–2232.
2. Aguilar-Rojas, A., Huerta-Reyes, M., Maya-Núñez, G., Arechavaleta-Velásco, F., Conn, P. M., Ulloa-Aguirre, A. and Valdés, J. (2012) Gonadotropin-releasing hormone receptor activates GTPase RhoA and inhibits cell invasion in the breast cancer cell line MDA-MB-231. *BMC Cancer* 12; 550.
3. Aman, A. and Piotrowski, T. (2008) Wnt/beta-catenin and Fgf signaling control collective cell migration by restricting chemokine receptor expression. *Dev. Cell* 15; 749–761.
4. Brábek, J., Mierke, C. T., Rösel, D., Veselý, P. and Fabry, B. (2010) The role of the tissue microenvironment in the regulation of cancer cell motility and invasion. *Cell Commun. Signal.* 8; 22.
5. Chrzanowska-Wodnicka, M. and Burridge, K. (1996) Rho-stimulated contractility drives the formation of stress fibers and focal adhesions. *J. Cell Biol.* 133; 1403–1415.
6. Fei, F., Zhang, D., Yang, Z., Wang, S., Wang, X., Wu, Z., Wu, Q. and Zhang, S. (2015) The number of polyploid giant cancer cells and epithelial-mesenchymal transition-related proteins are associated with invasion and metastasis in human breast cancer. *J. Exp. Clin. Cancer Res.* 34; 158.
7. Ferlay, J., Autier, P., Boniol, M., Heanue, M., Colombet, M. and Boyle, P. (2007) Estimates of the cancer incidence and mortality in Europe in 2006. *Ann. Oncol.* 18; 581–592.
8. Friedl, P. and Gilmour, D. (2009) Collective cell migration in morphogenesis, regeneration and cancer. *Nat. Rev. Mol. Cell Biol.* 10; 445–457.
9. Friedl, P., Locker, J., Sahai, E. and Segall, J. E. (2012) Classifying collective cancer cell invasion. *Nat. Cell Biol.* 14; 777–783.
10. Fritz, G., Just, I. and Kaina, B. (1999) Rho GTPases are overexpressed in human tumors. *Int. J. Cancer* 81; 682–687.
11. Fritz, G., Brachetti, C., Bahlmann, F., Schmidt, M. and Kaina, B. (2002) Rho GTPases in human breast tumours: expression and mutation analyses and correlation with clinical parameters. *Br. J. Cancer* 87; 635–644.
12. Gao, Z. H., Lu, C., Wang, M. X., Han, Y. and Guo, L. J. (2014) Differential β-catenin expression levels are associated with morphological features and prognosis of colorectal cancer. *Oncol. Lett.* 8; 2069–2076.
13. Gomez del Pulgar, T., Benitah, S. A., Valeron, P. F., Espina, C. and Lacal, J. C. (2005) Rho GTPase expression in tumourigenesis: evidence for a significant link. *Bioessays* 27; 602–613.
14. Graves, M. L., Cipollone, J. A., Austin, P., Bell, E. M., Nielsen, J. S., Gilks, C. B., McNagny, K. M. and Roskelley, C. D. (2016) The cell surface mucin podocalyxin regulates collective breast tumor budding. *Breast Cancer Res.* 18; 11.
15. Hanahan, D. and Weinberg, R. A. (2011) Hallmarks of cancer: the next generation. *Cell* 144; 676–674.
16. Heemskerk, N., Schimmel, L., Oort, C., van Rijssel, J., Yin, T., Ma, B., van Unen, J., Pitter, B., Huveneers, S., Goedhart, J., Wu, Y., Montanez, E., Woodfin, A. and van Buul, J. D. (2016) F-actin-rich contractile endothelial pores prevent vascular leakage during leukocyte diapedesis through local RhoA signalling. *Nat. Commun.* 7; 10493.
17. Jaffe, A. B. and Hall, A. (2005) Rho GTPases: biochemistry and biology. *Annu. Rev. Cell Dev. Biol.* 21; 247–269.
18. Jeon, M., Lee, J., Nam, S. J., Shin, I., Lee, J. E. and Kim, S. (2015) Induction of fibronectin by HER2 overexpression triggers adhesion and invasion of breast cancer cells. *Exp. Cell Res.* 333; 116–126.
19. Kalluri, R. and Weinberg, R. A. (2009) The basics of epithelial-mesenchymal transition. *J. Clin. Invest.* 119; 1420–1428.
20. Kanai, T., Yamanishi, T., Shirataki, H., Takagi, K., Asami, H., Ito, Y. and Yoshida, K. (2004) Overexpression of RhoA, Rac1, and Cdc42 GTPases is associated with progression in testicular cancer. *Clin. Cancer Res.* 10; 4799–4805.
21. Kennecke, H., Yerushalmi, R., Woods, R., Cheang, M. C., Voduc, D., Speers, C. H., Nielsen, T. O. and Gelmon, K. (2010) Metastatic behavior of breast cancer subtypes. *J. Clin. Oncol.* 28; 3271–3277.
22. Lin, H. H., Lin, H. K., Lin, I. H., Chiou, Y. W., Chen, H. W., Liu, C. Y., Harn, H. I., Chiu, W. T., Wang, Y. K., Shen, M. R. and Tang, M. J. (2015) Mechanical phenotype of cancer cells: cell softening and loss of stiffness sensing. *Oncotarget* 6; 20946–20958.
23. Macabeo-Ong, M., Ginzinger, D. G., Dekker, N., McMillan, A., Regezi, J. A., Wong, D. T. W. and Jordan, R. C. K. (2002) Effect of duration of fixation on quantitative reverse transcription polymerase chain reaction analysis. *Mod. Pathol.* 15; 979–987.
24. Maeda, T., Nakanishi, Y., Hirotani, Y., Fuchinoue, F., Enomoto, K., Sakurai, K., Amano, S. and Nemoto, N. (2016) Immunohistochemical co-expression status of cytokeratin 5/6, androgen receptor, and p53 as prognostic factors of adjuvant chemotherapy for triple negative breast cancer. *Med. Mol. Morphol.* 49; 11–21.
25. Mazieres, J., Antonia, T., Daste, G., Muro-Cacho, C., Berchery, D., Tillement, V., Pradines, A., Sebti, S. and Favre, G. (2004) Loss of RhoB expression in human lung cancer progression. *Clin. Cancer Res.* 10; 2742–2750.
26. Nakanishi, Y., Shimizu, T., Tsujino, I., Obana, Y., Seki, T., Fuchinoue, F., Ohni, S., Oinuma, T., Kusumi, Y., Yamada, T., Takahashi, N., Hashimoto, S. and Nemoto, N. (2013) Semi-nested real-time reverse transcription polymerase chain reaction methods for the successful quantitation of cytokeratin mRNA expression levels for the subtyping of non-small-cell lung

carcinoma using paraffin-embedded and microdissected lung biopsy specimens. *Acta Histochem. Cytochem.* 46; 85–96.
27. Nguyen, D. X., Bos, P. D. and Massagué, J. (2009) Metastasis: from dissemination to organ-specific colonization. *Nat. Rev. Cancer* 9; 274–284.
28. Orgaz, J. L., Herraiz, C. and Sanz-Moreno, V. (2014) Rho GTPases modulate malignant transformation of tumor cells. *Small GTPases* 5; e29019.
29. Pasquier, J., Abu-Kaoud, N., Abdesselem, H., Madani, A., Hoarau-Véchot, J., Thawadi, H. A., Vidal, F., Couderc, B., Favre, G. and Rafii, A. (2015) SDF-1alpha concentration dependent modulation of RhoA and Rac1 modifies breast cancer and stromal cells interaction. *BMC Cancer* 15; 569.
30. Provenzano, P. P., Inman, D. R., Eliceiri, K. W., Trier, S. M. and Keely, P. J. (2008) Contact guidance mediated three-dimensional cell migration is regulated by Rho/ROCK-dependent matrix reorganization. *Biophys. J.* 95; 5374–5384.
31. Rodriguez-Boulan, E. and Macara, I. G. (2014) Organization and execution of the epithelial polarity programme. *Nat. Rev. Mol. Cell Biol.* 15; 225–242.
32. Sahai, E. and Marshall, C. J. (2003) Differing modes of tumour cell invasion have distinct requirements for Rho/ROCK signaling and extracellular proteolysis. *Nat. Cell Biol.* 5; 711–719.
33. Shanker, J. and Nabi, I. R. (2015) Actin cytoskeleton regulation of epithelial mesenchymal transition in metastatic cancer cells. *PLoS One* 10; e0119954.
34. Sun, K., Duan, X., Cai, H., Liu, X., Yang, Y., Li, M., Zhang, X. and Wang, J. (2016) Curcumin inhibits LPA-induced invasion by attenuating RhoA/ROCK/MMPs pathway in MCF7 breast cancer cells. *Clin. Exp. Med.* 16; 37–47.
35. Thiery, J. P. (2002) Epithelial-mesenchymal transitions in tumour progression. *Nat. Rev. Cancer* 2; 442–454.
36. Torre, L. A., Bray, F., Siegel, R. L., Ferlay, J., Lortet-Tieulent, J. and Jemal, A. (2015) Global cancer statistics, 2012. *CA Cancer J. Clin.* 65; 87–108.
37. Vitorino, P. and Meyer, T. (2008) Modular control of endothelial sheet migration. *Genes Dev.* 22; 3268–3281.
38. Wang, X., Enomoto, A., Asai, N., Kato, T. and Takahashi, M. (2016) Collective invasion of cancer: Perspectives from pathology and development. *Pathol. Int.* 66; 183–192.
39. Watanabe, N., Nakanishi, Y., Kinukawa, N., Ohni, S., Obana, Y., Nakazawa, A. and Nemoto, N. (2014) Expressions of somatostatin receptor subtypes (SSTR-1, 2, 3, 4 and 5) in neuroblastic tumors; special reference to clinicopathological correlations with International Neuroblastoma Pathology Classification and outcomes. *Acta Histochem. Cytochem.* 47; 219–229.
40. Xiao, G., Wang, X., Wang, J., Zu, L., Cheng, G., Hao, M., Sun, X., Xue, Y., Lu, J. and Wang, J. (2015) CXCL16/CXCR6 chemokine signaling mediates breast cancer progression by pERK1/2-dependent mechanisms. *Oncotarget* 6; 14165–14178.
41. Yu, M., Bardia, A., Wittner, B. S., Stott, S. L., Smas, M. E., Ting, D. T., Isakoff, S. J., Ciciliano, J. C., Wells, M. N., Shah, A. M., Concannon, K. F., Donaldson, M. C., Sequist, L. V., Brachtel, E., Sgroi, D., Baselga, J., Ramaswamy, S., Toner, M., Haber, D. A. and Maheswaran, S. (2013) Circulating breast tumor cells exhibit dynamic changes in epithelial and mesenchymal composition. *Science* 339; 580–584.